NASA
Technical Memorandum 100141

AVSCOM
Technical Report 87-C-25

Design and Performance of Controlled-Diffusion Stator Compared With Original Double-Circular-Arc Stator

Thomas F. Gelder, James F. Schmidt, and Kenneth L. Suder
Lewis Research Center
Cleveland, Ohio

and

Michael D. Hathaway
Propulsion Directorate
U.S. Army Aviation Research and Technology Activity—AVSCOM
Lewis Research Center
Cleveland, Ohio

(NASA-TM-100141) DESIGN AND PERFORMANCE OF CONTROLLED-DIFFUSION STATOR COMPARED WITH ORIGINAL DOUBLE-CIRCULAR-ARC STATOR (NASA) 22 p Avail: NTIS HC A02/MF A01 CSCL 21E

N87-26910

Unclas
G3/07 0092891

Prepared for the
1987 Aerospace Technology Conference and Exposition
sponsored by the Society of Automotive Engineers
Long Beach, California, October 5-8, 1987

NASA

DESIGN AND PERFORMANCE OF CONTROLLED-DIFFUSION STATOR COMPARED WITH ORIGINAL DOUBLE-CIRCULAR-ARC STATOR

Thomas F. Gelder, James F. Schmidt, and Kenneth L. Suder
National Aeronautics and Space Administration
Lewis Research Center
Cleveland, Ohio 44135

and

Michael D. Hathaway
Propulsion Directorate
U.S. Army Aviation Research and Technology Activity - AVSCOM
Lewis Research Center
Cleveland, Ohio 44135

SUMMARY

The capabilities of a stator blade row having controlled-diffusion (CD) blade sections were compared with the capabilities of a stator blade row having double-circular-arc (DCA) blade sections. A CD stator with the same chord length but half the blades of the DCA stator was designed and tested. The same fan rotor (tip speed, 429 m/sec; pressure ratio, 1.65) was used with each stator row. The design and analysis system is briefly described here. The overall stage and rotor performances with each stator are then compared along with selected blade element data. The CD stator had approximately a 1 percentage point greater minimum overall efficiency decrement than the DCA stator at or near design speed.

E-3694-1

NOMENCLATURE

C_p static pressure coefficient, $\frac{p_s - p_2}{\left(\frac{\gamma - 1}{2}\right) p_2 M_2^2}$

H_1 incompressible form factor (ref. 15)*

M Mach number

m meridional streamline distance

N_D design speed of rotor

P total pressure

p static pressure

r radius from axis of rotation

*Numbers in parentheses designate references at end of paper.

T total temperature

w weight flow corrected to standard day conditions at station 1 (fig. 3)

β absolute air angle

β^*_{LE} blade mean line angle at leading edge

γ ratio of specific heats for air, 1.40

δ^* boundary-layer displacement thickness (ref. 15)

η_{ad} stage or rotor adiabatic efficiency, $\dfrac{\left(\dfrac{\bar{P}_3}{\bar{P}_1}\right)^{\frac{\gamma-1}{\gamma}} - 1}{\left(\dfrac{\bar{T}_3}{\bar{T}_1}\right) - 1}$ or $\dfrac{\left[\dfrac{(P_3)_{3hi}}{P_1}\right]^{\frac{\gamma-1}{\gamma}} - 1}{\left(\dfrac{\bar{T}_3}{\bar{T}_1}\right) - 1}$

$\Delta\eta$ efficiency decrement across stator, equals rotor η_{ad} minus stage η_{ad}

θ angular coordinate

σ solidity, blade chord to spacing ratio

$\bar{\omega}_w$ stator loss coefficient (wake), $\dfrac{(P_3)_{3hi} - \bar{P}_3}{P_2 - p_2}$, ref. 17

Subscripts:

choke with stage choked at design speed

s stator surface

1 instrumentation station upstream of rotor (fig. 3)

2 instrumentation station between rotor and stator (fig. 3)

3 instrumentation station downstream of stator (fig. 3)

3hi arithmetic average of three highest values measured across stator gap

Superscript:

- mass-averaged value

INTRODUCTION

Various blade cross-sectional shapes have been studied in order to improve fan or compressor efficiency and flow range and to achieve the same performance with fewer but more highly loaded blades. Airfoil shapes that control the diffusion of velocity over the surface can increase the amount of laminar flow in relation to turbulent flow and delay or avoid flow separation before the trailing edge. Controlled-diffusion airfoil shapes can improve the airfoil's operating efficiency and have found wide application in recent years. Some examples have been isolated, supercritical airfoils (ref. 1), supercritical cascades (refs. 2 to 5), subcritical stators for compressors (ref. 6), and low-speed turning vanes for wind tunnels (refs. 7 and 8). Although controlled-diffusion (CD) shapes are more complex then double-circular-arc (DCA) shapes, modern numerically controlled machining techniques should reduce difficulties in fabrication. Aerodynamic loadings (or turnings) can be higher with CD blade shapes than with conventional shapes without sacrificing loss levels or operating range (ref. 9). This capability can reduce the number of blades required in a conventional fan stator row.

The objective of this study was to compare the capabilities of a stator blade row having CD blade sections with the capabilities of one having DCA blade sections. A CD stator with the same chord length as the DCA stator (ref. 10) but with half the blades was designed and tested. The same fan rotor (tip speed, 429 m/sec; pressure ratio, 1.65) was used with each stator row. One-half the stator blade count was selected because (1) the stator blade element flow predictions for such a design indicated some chance of success, (2) the capabilities of the controlled-diffusion blading in a real flow environment could be dramatically demonstrated, and (3) existing casings for the stage could be reused. A CD stator design with the same blade number and chord length as the DCA stator was considered for the present comparative study. However, that choice was rejected because little or no measurable improvement in performance was expected over the original DCA design, which had performed very well.

This paper briefly describes the design and analysis system for the CD stators. The overall stage and rotor performances with each stator are then compared, as are selected blade element data from each stator. Measurements of chordwise distributions of static pressure at 10-, 50-, and 90-percent CD stator spans are discussed. The performance data presented can be used to assess the design and analysis system. A data base for the evaluation of other computational codes is also provided.

DESIGN AND ANALYSIS SYSTEM

The design and analysis system used for the CD stator blade row is diagrammed in figure 1. It is a quasi-three-dimensional, inviscid-viscous interaction system. Only the overall process is described here; details of the individual codes are contained in the references cited. The compressor design program (CDP code, (ref. 11)) first made a hub-to-tip plane flow-field calculation (axisymmetric) with preliminary blade geometry that satisfied the desired velocity diagrams at the blade edges. The CDP and MERIDL codes (ref. 12) use previous test results from the original stage at peak efficiency operation to set the bounding flow conditions for the CD stator. The CDP code did not calculate flow conditions within the blade rows. The flow within and

around the stator row was analyzed by MERIDL, TSONIC (ref. 13), QSONIC (ref. 14), and BLAYER (ref. 15). If the desired results were not achieved, new stator blade cross sections were generated by the blade element program (BEP), which is part of the CDP code.

The analysis procedure was as follows: First, the inlet and outlet Mach numbers and air angles, along with streamtube convergence and radius change, were determined by MERIDL. Next, individual blade element cross-sectional geometry was generated by the BEP. With this blade geometry and bounding flow conditions, blade-to-blade flow fields were calculated for selected spanwise sections by using the TSONIC and QSONIC codes. Although results from these two codes were essentially the same over most of the chord length, there were differences near both the leading and trailing edges. The QSONIC code provides better definition near the leading edge than does the TSONIC code, and it is more accurate when local velocities are supersonic. The TSONIC code, however, provides more realistic velocities near the trailing edge than does the QSONIC. TSONIC employs a mass injection routine at the trailing edge that simulates the blade wake (unpublished addendum to ref. 13). Thus, a composite of results was used with QSONIC values over the forward half-chord (approximately) and TSONIC values over the rear half-chord.

Because the code results from MERIDL, BEP, TSONIC, and QSONIC assume an inviscid flow, boundary-layer calculations were made next. The BLAYER code (ref. 15), with its two-dimensional integral method, calculates both laminar and turbulent boundary layers. The surface velocity distributions required as input to BLAYER were from the previous TSONIC and QSONIC results. From an initial laminar boundary layer at the leading edge, the BLAYER calculation proceeded chordwise until laminar separation was assumed to occur near the start of any adverse pressure gradient. A turbulent layer was then started by using initial conditions based on a laminar separation bubble model (ref. 16). To determine whether the turbulent layer would separate before the trailing edge, the incompressible form factor H_1 was continuously calculated. If the value of H_1 was less than 2.0, separation of the turbulent layer was not expected and the stator blade cross-sectional profile was acceptable. If H_1 was greater than 2.0, the profile was modified and the analysis procedure was repeated. The calculated boundary-layer displacement thickness δ^* was added to the blade profile for the TSONIC and QSONIC calculations. Blade sections at five spanwise locations (10-, 30-, 50-, 70-, and 90-percent spans) were designed in a similar fashion. These were then stacked in the CDP to make a blade. Geometries for any intermediate cross sections of interest were obtained from a simple CURVFIT routine. Next, a check was made to ensure the gross compatibility of the hub-to-tip and blade-to-blade solutions. Only a few iterations were required to match the boundary conditions for these codes.

As previously indicated, design flow conditions into and out of the CD stator were obtained from MERIDL. The MERIDL nongeometric input consisted of radial profiles of inlet and outlet total pressure and tangential velocity along with inlet total temperature. These aerodynamic values were obtained from previous measurements. The total pressure profiles input to MERIDL were faired to decrease close to the walls in order to simulate the effect of the wall boundary-layer blockage. It was assumed that this fairing would serve in place of specifying wall blockage factors.

Finally, structural analysis was conducted before fabrication coordinates were released. Whenever design criteria were not met, the blade geometry was changed and the process retraced as indicated in figure 1.

The CD stator (S67B) blade cross section at 50-percent span that resulted from this design and analysis system is shown in figure 2. (Coordinates for the CD stator cross sections at the 10-, 50-, and 90-percent spans are given in table I.). For comparison, the original DCA stator (S67) blade is also shown. Midspan solidity σ is 0.84 for S67B and 1.68 for S67. The CD stator turns most of the air over the forward half-chord. The relatively straight rear half of the blade is necessary to prevent turbulent boundary-layer separation. In contrast, the DCA (S67) blade has a constant turning rate from the leading edge to the trailing edge. Both stators are designed to turn the flow to the axial direction. Another major difference in the two blade shapes is the angle made by the mean line of the blade with the oncoming flow at the leading edge. This incidence angle is almost 0° for S67 (the DCA blade) but near -14° for S67B (the CD blade). This large negative incidence angle for S67B was necessary to avoid the tendency for a suction surface velocity spike near the leading edge. Such a spike could trigger premature laminar boundary-layer separation followed by a relatively thick reattached turbulent layer that could in turn separate prematurely. Although only midspan stator shapes are shown in figure 2, four other CD sections from hub to tip were designed and stacked for the final blade. The other sections have similar features but differ in total turning and solidity as required across the span.

APPARATUS AND PERFORMANCE CALCULATIONS

The flow path and the instrumentation locations for the single-stage fan are shown in figure 3. The original stage (ref. 10) utilized DCA blading for both the rotor (R67) and the stator (S67). The controlled-diffusion stator with 17 blades is called stator 67B (S67B). Aerodynamic data were obtained from the traverse of conventional pneumatic probes (ref. 17) at the three measuring stations indicated. Chordwise distributions of static pressure were also measured on the CD stator at 10-, 50-, and 90-percent spans (design streamline locations at the rotor trailing edge). Local surface Mach number were determined from static pressures and the corresponding stator inlet total pressure measured at station 2.

Overall stage performance was calculated from mass-averaged total pressures and total temperatures measured at stations 1 and 3. Stator loss coefficients $\bar{\omega}_w$ utilized an average of the three highest total pressures measured across a stator gap at station 3 to represent the upstream pressure reference in its numerator (see NOMENCLATURE). The same three-high average was also used for rotor outlet pressure. Mass-averaged total temperatures from station 3 were used in determining rotor energy addition and rotor efficiency. In reducing and evaluating the present data, the station 2 measurements were used for air angle, Mach number, and the difference between total and static pressure that forms the denominator of $\bar{\omega}_w$.

RESULTS AND DISCUSSION

Overall performances of rotor 67 (R67), stage 67 (R67 with the DCA stator, S67), and stage 67B (R67 with the CD stator, S67B) are discussed first. The CD

stator blade surface data for the tip, mean, and hub sections are then examined in some detail. Finally, blade element losses from the CD and DCA stator rows are compared.

Overall performance. - Rotor 67, stage 67, and stage 67B overall performance values are presented in figure 4. The left side of each figure part shows stator 67B related data; the right side shows stator 67 related data. Data at three speeds near design are shown, and the independent variable for all parts is the weight flow ratioed to the choked value at design speed. Such a weight-flow ratio is used to minimize the effect of small absolute flow differences that may arise from other installations of the same hardware in the same test facility.

As indicated on the left side of figure 4(a), rotor 67 added slightly different amounts of energy (represented by $\overline{T_3/T_1}$ at 90 to 100 percent of design speed N_D) depending upon which stator (67B or 67) followed it. With stator 67B, rotor 67 added slightly more energy at 100-percent N_D and slightly less at 90- and 95-percent N_D. The rotor total pressure ratios $(P_3)_{3hi}/P_1$ followed these differences in energy added and are indicated by the solid symbols in figure 4(b). The rotor efficiencies (fig. 4(c)) were essentially the same with either stator. The small efficiency differences indicated are probably not significant because installation differences or measurement inaccuracies might easily account for them. Rotor peak efficiency tended to decrease with increasing speed from 90- to 100-percent N_D. Higher shock losses for this rotor (design tip speed, 429 m/sec) are probably responsible for this. The performance differences for rotor 67 operating with either stator are small, and some are mixed even within the narrow speed range shown. With the relatively large axial spacing between rotor and stator (fig. 3), only small interaction effects were anticipated.

The stage total pressure ratios ($\overline{P_3/P_1}$, fig. 4(b)) were generally somewhat lower for stage 67B than for stage 67, primarily because of the difference in stator performance. The near-stall lines were essentially the same for both stages, suggesting that stage stall was initiated by the rotor used for both stages. Previous rotor-alone tests at design speed (ref. 18) indicated stall at about the same weight flow shown in figure 4(b) for the stage. This supports the conclusion that the rotor initiated stall for both stages.

The difference between overall efficiencies of the rotor and stage is one measure of overall stator performance. The minimum values of these overall efficiency decrements across the stators provided a useful basis for comparing the performances of different stator designs. As indicated (fig. 4(d)), the stator 67B minimum efficiency decrement was nearly the same for 90-, 95-, and 100-percent N_D, with an average value of 0.038. A comparable speed-averaged value for stator 67 was 0.028. Thus, there was approximately a 1-percentage-point increase in minimum overall efficiency decrement for the CD stator (S67B) relative to the DCA stator (S67) at speeds near design. The reasons for this difference are developed next by examining the stator surface Mach number and pressure coefficient distributions.

Surface distributions for CD stator. - Local surface Mach number distributions obtained at the operating point nearest that for the minimum efficiency decrement across the stator at 100-percent N_D are shown in figure 5. The predicted distributions from the analysis codes (TSONIC and QSONIC) are also

shown, along with tabulated conditions of weight flow ratio w/w_{choke}, inlet Mach number M_2, inlet air angle β_2, and stator loss coefficient $\bar{\omega}_w$.

For the operating point indicated on figure 5, the measured inlet Mach numbers were about 10 percent higher than design. This accounts in part for the upward shift in the Mach number distributions relative to the predictions at all three spanwise locations. Insufficient accounting for wall boundary-layer blockage in MERIDL caused the inlet Mach numbers to be underpredicted. This in turn led to predicting inlet air angles that were several degrees too high. Depending on the spanwise location, the measured inlet air angles were 3.1° to 4.1° less than predicted (fig. 5). Thus simulating the effect of wall boundary-layer blockage by fairing the total pressure profiles input to MERIDL so that they decreased close to the walls was not adequate. Realistic wall blockage factors were needed instead.

At 50-percent span (fig. 5), the whole Mach number pattern was shifted upward from prediction, but the gradients were similar. In particular the Mach numbers on the suction surface continued to decrease until near the trailing edge. This indicated little or no boundary-layer separation. The low measured loss coefficient $\bar{\omega}_w$ of 0.029 supported this observation. At 10-percent span, $\bar{\omega}_w$ was 0.058, double that at midspan. The suction surface Mach number gradients also differed, with a departure from prediction starting near midchord. Such departures suggested a separating boundary layer. A lower design loss level was also suggested if separation could be avoided. The highest losses were in the hub region (90-percent span), where $\bar{\omega}_w$ was 0.131, about 50 percent higher than expected. Here also the suction surface Mach number gradients departed from prediction, starting at about 0.4 chord. The losses near the hub were much higher than those near the tip even though their suction surface Mach number gradients were similar. This is discussed later.

At 90-percent N_D, the measured inlet Mach numbers M_2 were close to the original design and analysis predictions (fig. 6). The suction surface Mach number levels and gradients were close to predictions near the stator's minimum efficiency decrement. Both tip (10-percent span) and mean (50-percent span) sections displayed nonseparated surface gradients all the way to the trailing edge. The measured loss coefficient for the tip was improved to 0.047, but for the mean it remained at 0.030. Only the hub (90-percent span) section continued to show a premature separation on the suction surface and a high loss coefficient of 0.140.

A comparison of tip-section performance between figures 5 and 6 indicates its high sensitivity to inlet air angle. A decrease in β_2 of about 2° (32.3° to 30.4°) eliminated the premature separation (fig. 5), which in turn reduced $\bar{\omega}_w$ from 0.058 to 0.047. As shown later (fig. 10), it was the decrease in β_2 rather than the decrease in M_2 that reduced the loss here.

Comparisons were made between the predicted and actual surface pressure coefficient distributions for the tip, mean, and hub sections when each was operating nearest its design β_2 (fig. 7). The closest β_2 matches (data versus design) involved data for three operating speeds (90-, 95-, and 100-percent N_D). This presented no problem when comparing static pressure coefficients C_p because M_2^2 appears in C_p's denominator. At design values

of β_2, there was a similar C_D pattern for all sections. The suction surface indicated a short, relatively flat coefficient near the leading edge. This was followed by an adverse pressure gradient that indicated premature separation around midchord. The accompanying loss coefficients $\overline{\omega}_w$ were all relatively high: 0.070 for the tip, 0.089 for the mean, and 0.144 for the hub. Relatively high losses also occurred in cascade tests of a similar CD stator section design (ref. 4) when similar indications of separation starting near midchord were measured for some inlet flow conditions. At those conditions, flow visualization studies (ref. 4) revealed a rather large laminar separation bubble in the forward chord region with a flattened pressure distribution beneath it. The reattached, turbulent boundary layer following such a bubble was believed to be substantially thickened and therefore less able to negotiate an adverse pressure gradient without separation. (A corner suction slot starting in the region of reattachment precluded an observation of this boundary-layer thickness.) Similar boundary-layer behavior is attributed to the results shown in figure 7.

It appeared that premature separation of the laminar boundary layer, with perhaps a large separation bubble before a thick turbulent layer reattaches on the suction surface, should be avoided for low-loss operation. To emphasize this point, a mean-section surface Mach number distribution at design speed and near-design β_2 was compared with one near minimum-loss β_2 (fig. 8). The dashed lines are predictions from the blade-to-blade codes (refs. 13 and 14).

The significantly different surface Mach number patterns in figure 8 are the result of a 3 8° difference in inlet air angle. At a β_2 of 35.6° (fig. 8(b)) there was a strong, favorable pressure gradient on the suction surface from the leading edge to about 40-percent chord. Thus, over this region, a thin, laminar boundary layer was maintained. There was no local flattening of the surface Mach numbers such as accompanied the laminar separation bubbles observed in the tests described by Boldman (ref. 4). Over the last 60 percent of chord, a strong, adverse pressure gradient existed. Because there was little departure from the calculated Mach number distribution there, a turbulent boundary layer that starts relatively thin a little beyond 40-percent chord is envisioned. The difference in loss coefficient between the surface Mach number patterns at near-design and minimum-loss β_2 was a factor of 3, 0.029 (fig. 8(b)) compared with 0.089 (fig. 8(a)).

For the low-loss, unseparated condition (fig. 8(b)), the blade surface Mach numbers calculated by the blade-to-blade codes agreed well with the data when the input boundary values such as M_2 and β_2 were the same as those measured. However, the BLAYER calculations using the original inviscid prediction (fig. 8(a)) did not predict the early laminar separation experienced, even though a generally favorable pressure gradient to about 35-percent chord was indicated. On the basis of present data and similar results from cascade testing of other CD blade sections (refs. 3 and 19), a continuously strong, favorable gradient to about 35- to 40-percent chord is recommended for highly loaded blades in order to avoid premature laminar separation and consequent premature turbulent separation and high loss.

At all operating conditions (figs. 5 to 7), the hub section (90-percent span) of stator 67B showed turbulent boundary-layer separation from the suction surface around midchord. The relatively poor performance over the one-third span nearest the hub caused the minimum overall efficiency decrement across the stator to be approximately 1 percentage point higher for S67B than for S67 at

speeds of 90- to 100-percent N_D. Thus, it is instructive to further examine the surface Mach number distributions near the hub and compare them with those at midspan, where the performance was good, at least for some inlet air angles (fig. 9). The Mach number patterns over the forward one-third chord of the suction surface were similar for both the hub and mean sections. However, the Mach number distribution for the hub section indicated a flow separation near 50-percent chord, whereas no flow separation was apparent for the mean section. The corresponding loss coefficients were much different, being 0.159 for the hub but only 0.029 for the mean.

Premature separation of the hub-section boundary layer occurred at all speeds and flows tested. These included conditions that resulted in low levels of diffusion factor (defined by Johnsen (ref. 20, p. 203). A strongly favorable Mach number gradient was achieved over approximately the first one-third chord of the hub section (fig. 9). However, this was not sufficient to avoid premature turbulent boundary-layer separation as it was for the mean section. (As noted earlier (Fig. 6), such favorable forward-chord distributions also prevented early turbulent separation from the tip section.) Thus, non-two-dimensional flow effects in the hub end-wall region are thought to be responsible. A corner stall (between stator blade suction surface and hub end wall) or secondary or crossflows in the hub end-wall region are two possible flow mechanisms. Therefore, a simple redesign of the two-dimensional blade sections near the hub is not likely to improve their performance. What is needed instead is a redesign that minimizes or eliminates a possible corner stall or reduces crossflows in the hub region. Such a redesign could include changes to the rotor, the inner-wall contour, or the stator.

When the stator blade number was cut in half for stator 67B (with the same air-turning requirements as for stator 67), the blade-loading and crossflow gradients were doubled. Also, with only half the blades, there was twice the amount of lower energy flow along the hub wall per blade passage. To improve the hub region flow by stator redesign, two changes are suggested. The first is to increase the number of blades moderately, and the second is to reduce the chord length, at least in the hub region (ref. 17).

Summary of stator blade losses. - Loss coefficients $\overline{\omega}_w$ for stators 67B and 67 are presented (fig. 10) as a function of inlet air angle β_2 and for three spanwise locations near the tip, mean, and hub. Data at 90-, 95-, and 100-percent N_D yielded essentially the same results, and all were used to draw the faired lines shown. At midspan, the minimum loss coefficient was approximately 0.025 for each stator and occurred at about the same β_2. Near the tip, the minimum loss for S67B was approximately 0.03, compared with approximately 0.04 for S67. Near the hub, the minimum loss was much higher for S67B (0.135 compared with 0.07). Stator blade incidence angles can be obtained (within 1°) by subtracting the value of the blade mean line angle at the leading edge β^*_{LE} given on each part of figure 10 from the value of β_2 on the abscissa.

The inlet air angle range at low loss levels was wider for the lower-loaded stator 67. But a narrow, low loss range is not believed to be inherent in all more highly loaded CD blade designs. Here however, an equal low loss range for a CD blade with twice the loading of a well-designed, moderately loaded DCA blade is probably not achievable.

Figure 11 shows the spanwise distributions of losses for stators 67B and 67 when each blade row was operating at its minimum overall efficiency decrement at 90- to 100-percent N_D. The lines represent faired values of loss coefficient data such as that shown in figure 10, plus values from similar data plots for the 30- and 70-percent spans. The difference in loss levels between the two stator designs was primarily over the one-third span nearest the hub. There the losses differed increasingly as the inner wall was approached, with a factor of 2 indicated near 90-percent span. As previously indicated, the difference in overall stator efficiency decrement was 0.010.

When either of the stators was operating near its minimum overall efficiency decrement (fig. 11), the stator exit air angles at station 3 (fig. 3) were near the design intent of 0° at midspan for both stators. The exit air angle near either end wall was approximately 5° higher than design (underturned) for the CD stator and near 0° for the DCA stator. Thus, the much higher solidity of the DCA design provided better flow guidance in the end-wall regions than did the present CD design.

CONCLUDING REMARKS

The data presented here provide a base for evaluating a variety of computational codes. They include for the CD stator the surface Mach number distributions, inlet and exit conditions, loss values, blade cross-sectional geometries, and flow-path dimensions. These data are from the real flow environment following a rotor, and they include results at spanwise locations near the tip, mean, and hub. Additional insight for code evaluation may also be gained from recently published laser anemometer data for the midspan region of the same CD and DCA stators (refs. 21 and 22). Similar flow-field measurements have also been published for rotor 67 operating without a stator (refs. 18 and 23).

SUMMARY OF RESULTS

The design and steady-state aerodynamic performances of a fan stator row for a transonic single-stage fan with controlled-diffusion (CD) blade sections were presented. Comparisons were made with the originally designed double-circular-arc (DCA) stator row, which had twice the number of blades of equal chord. In addition to the usual traverse data upstream and downstream of the rotor and stator, chordwise distributions of surface Mach numbers from static taps on the CD stator at 10-, 50-, and 90-percent spans were also presented. The following principal results were obtained from these data:

1. The two-dimensional performances of the CD and DCA stators were similar, with minimum loss coefficients of about 0.030, except in the one-third span near the hub. In that area, the CD stator losses were much higher because of increased end-wall effects. Attaining the low two-dimensional loss performance with the CD blade sections under study required a strong, favorable, pressure gradient on the suction surface from the leading edge to about 35- to 40-percent chord.

2. Because of higher hub region losses, the CD stator had approximately a 1 percentage point greater minimum overall efficiency decrement than the DCA

stator at speeds from 90 to 100 percent of design. This was caused by higher hub region losses. Stage stall flows were unchanged by stator design.

REFERENCES

1. F. Bauer, P.R. Garabedian, and D. Korn, "Supercritical Wing Sections." Vol. I, II, and III, New York: Springer-Verlag, 1972, 1975, 1977.

2. H.E. Stephens, "Application of Supercritical Airfoil Technology to the Compressor Cascades." AIAA Paper 78-1138, July 1978.

3. H. Rechter, P. Schimming, and H. Starken, "Design and Testing of Two Supercritical Compressor Cascades." ASME Paper 79-GT-11, Mar. 1979.

4. D.R. Boldman, A.E. Buggele, and L.M. Shaw, "Experimental Evaluation of Shockless Supercritical Airfoils in Cascade." AIAA Paper 83-003, Jan. 1983. (NASA TN-83045.)

5. J.F. Schmidt, T.F. Gelder, and L.F. Donovan, "Redesign and Cascade Tests of a Supercritical Controlled Diffusion Stator Blade-Section." AIAA Paper 84-1207, June 1984. (NASA TM-83635.)

6. R.F. Behlke, J.D. Brooky, and E. Canal, "Study of Controlled Diffusion Stator Blading." (PWA-5698-77, Pratt & Whitney Aircraft Group) NASA CR-167995, 1983.

7. J.M. Sanz, E.R. McFarland, N.L. Sanger, T.F. Gelder, and R.H. Cavicchi, "Design and Performance of a Fixed, Nonaccelerating Guide Vane Cascade That Operates Over an Inlet Flow Angle Range of 60 Deg," Journal of Engineering for Gas Turbines and Power, Vol. 107, No. 2, Apr. 1985, pp. 477-484.

8. T.F. Gelder, R.D. Moore, J.M. Sanz, and E.R. McFarland, "Wind Tunnel Turning Vanes of Modern Design." AIAA Paper 86-0044, Jan. 1986. (NASA TM-87146.)

9. R.F. Behlke, "The Development of a Second Generation of Controlled Diffusion Airfoils for Multistage Compressors." Journal of Turbomachinery, Transactions of ASME, Vol. 108, No. 1, July 1986, pp. 32-41.

10. D.C. Urasek, W.T. Gorrell, and W.S. Cunnan, "Performance of Two-Stage Fan Having Low-Aspect-Ratio, First-Stage Rotor Blading." NASA TP-1493, 1979.

11. J.E. Crouse and W.T. Gorrell, "Computer Program for Aerodynamic and Blading Design of Multistage Axial-Flow Compressors," NASA TP-1946, 1981.

12. T. Katsanis and W.D. McNally, "Revised Fortran Program for Calculating Velocities and Streamlines on the Hub-Shroud Midchannel Stream Surface of an Axial-, Radial-, or Mixed-Flow Turbomachine or Annular Duct. I: Users Manual." NASA TN D-8430, 1977.

13. T. Katsanis, "Fortran Program for Calculating Transonic Velocities on a Blade-to-Blade Stream Surface of a Turbomachine." NASA TN D-5427, 1969.

14. C.A. Farrell, "Computer Program for Calculating Full Potential Transonic Quasi-Three-Dimensional Flow Through a Rotating Turbomachinery Blade Row." NASA TP-2030, 1982.

15. W.D. McNally, "Fortran Program for Calculating Compressible Laminar and Turbulent Boundary Layers in Arbitrary Pressure Gradients." NASA TN D-5681, 1970.

16. W.B. Roberts, "The Effect of Reynolds Number and Laminar Separation on Axial Cascade Performance." Journal of Engineering for Power, Vol. 97, No. 2, Apr. 1975, pp. 261-274.

17. T.F. Gelder, "Aerodynamic Performances of Three Fan Stator Designs Operating With Rotor Having Tip Speed of 337 Meters per Second and Pressure Ratio of 1.54. I - Experimental Performance." NASA TP-1610, 1980.

18. A.J. Strazisar, "Investigation of Flow Phenomena in a Transonic Fan Rotor Using Laser Anemometry." Journal of Engineering for Gas Turbines and Power, Vol. 107, No. 2, Apr. 1985, pp. 427-435.

19. H.E. Stephens and D.E. Hobbs, "Design and Performance Evaluation of Supercritical Airfoils for Axial Flow Compressors," Pratt & Whitney Aircraft Report PWA-FR-11455, June 1979. (Avail. NTIS, AD-A071206.)

20. Irving A. Johnsen and Robert O. Bullock, eds.: "Aerodynamic Design of Axial-Flow Compressors." NASA SP-36, 1965.

21. K.L. Suder, M.D. Hathaway, T.H. Okiishi, A.J. Strazisar, and J.J. Adamczyk, "Measurements of the Unsteady Flow Field Within the Stator Row of a Transonic Axial Flow Fan. I - Measurement and Analysis Technique." ASME Paper 87-GT-226, June 1987. (NASA TM-88945.)

22. M.D. Hathaway, K.L. Suder, T.H. Okiishi, A.J. Strazisar, and J.J. Adamczyk, "Measurements of the Unsteady Flow Field Within the Stator Row of a Transonic Axial Flow Fan. II - Results and Discussion," ASME Paper 87-GT-227, June 1987. (NASA TM-88946.)

23. M.H. Pierzga and J.R. Wood, "Investigation of the Three-Dimensional Flow Field Within a Transonic Fan Rotor: Experiment and Analysis." Journal of Engineering for Gas Turbines and Power, Vol. 107, No. 2, Apr. 1985, pp. 436-449.

TABLE I. - METAL COORDINATES FOR STATOR 67B AT 10-, 50-, AND 90-PERCENT SPANS

Location, percent of span	Upper surface		Lower surface	
	Meridional streamline distance, m, cm	Tangential distance, r(θ), cm	Meridional streamline distance, m, cm	Tangential distance, r(θ), cm
10 (tip)	0.0143	0.0437	0.0875	-0.0162
	.0823	.1408	.1698	.0627
	.1945	.2801	.2987	.1719
	.3594	.4518	.4788	.3075
	.5840	.6465	.7132	.4631
	.8723	.8542	1.0058	.6336
	1.1753	1.0382	1.3061	.7905
	1.4900	1.2028	1.6133	.9330
	1.8148	1.3847	1.9257	1.0607
	2.1510	1.4654	2.2430	1.1700
	2.4990	1.5551	2.5643	1.2584
	2.8535	1.6069	2.8919	1.3279
	3.2083	1.6266	3.2260	1.3793
	3.5607	1.6236	3.5656	1.4142
	3.9100	1.6075	3.9091	1.4356
	4.2578	1.5865	4.2541	1.4449
	4.6049	1.5660	4.5991	1.4414
	4.8945	1.5501	4.8859	1.4251
	5.1273	1.5366	5.1133	1.3096
	5.3032	1.5241	5.2813	1.3707
	5.5464	1.5010	5.5464	1.3063
50 (mean)	0.0082	0.0311	0.0734	-0.0202
	.0698	.1343	.1594	.0570
	.1756	.2812	.2914	.1691
	.3344	.4644	.4724	.3077
	.5514	.6696	.7053	.4750
	.8288	.8953	.9903	.6679
	1.1198	1.1024	1.2817	.8538
	1.4240	1.2947	1.5773	1.0273
	1.7428	1.4675	1.8797	1.1855
	2.0772	1.6127	2.1897	1.3184
	2.4262	1.7218	2.5082	1.4271
	2.7843	1.7930	2.8349	1.5169
	3.1449	1.8251	3.1699	1.5828
	3.5034	1.8300	3.5122	1.6277
	3.8591	1.8203	3.8588	1.6569
	4.2123	1.7985	4.2081	1.6666
	4.5647	1.7768	4.5577	1.6615
	4.8585	1.7558	4.8478	1.6392
	5.0941	1.7377	5.0777	1.6079
	5.2718	1.7246	5.2477	1.5767
	5.5126	1.6978	5.5126	1.5056
90 (hub)	0.0043	0.0230	0.0719	-0.0177
	.0542	.1391	.1527	.0716
	.1451	.3042	.2771	.1996
	.2859	.5099	.4484	.3639
	.4807	.7486	.6681	.5660
	.7300	1.0190	.9345	.8064
	.9933	1.2762	1.2030	1.0427
	1.2728	1.5201	1.4761	1.2680
	1.5734	1.7447	1.7581	1.4736
	1.8992	1.9417	2.0522	1.6515
	2.2558	2.0899	2.3594	1.8018
	2.6231	2.1863	2.6859	1.9241
	2.9919	2.2390	3.0267	2.0204
	3.3592	2.2728	3.3769	2.0979
	3.7240	2.2887	3.7326	2.1493
	4.0880	2.2985	4.0913	2.1808
	4.4519	2.3038	4.4507	2.1914
	4.7555	2.3034	4.7491	2.1832
	4.9993	2.2970	4.9862	2.1638
	5.1828	2.2867	5.1618	2.1410
	5.4132	2.2627	5.4132	2.0918

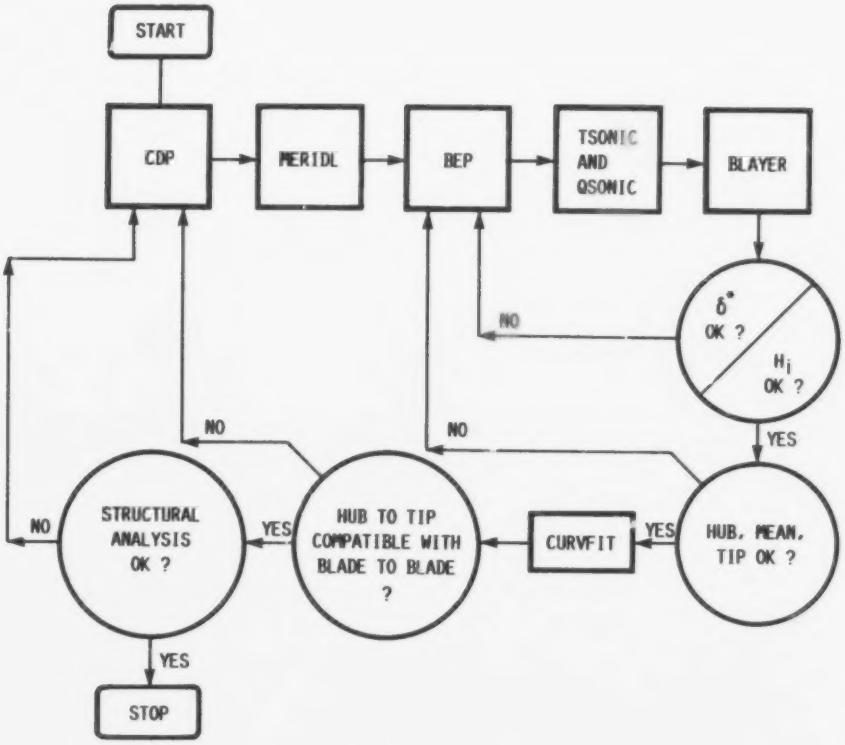

FIGURE 1. - DESIGN AND ANALYSIS SYSTEM.

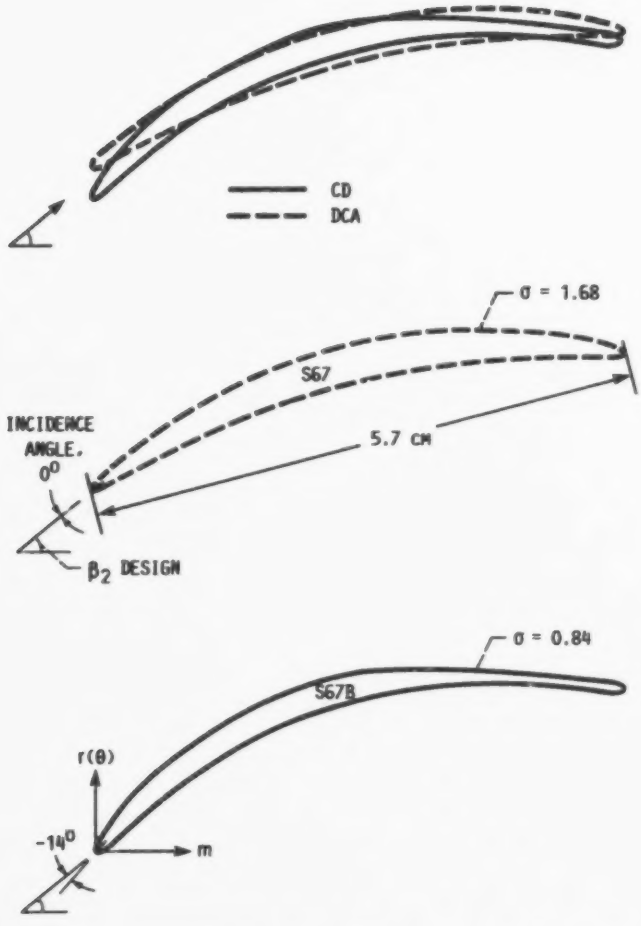

FIGURE 2. - CROSS SECTIONS OF STATORS 67B AND 67 AT 50-PERCENT SPAN.

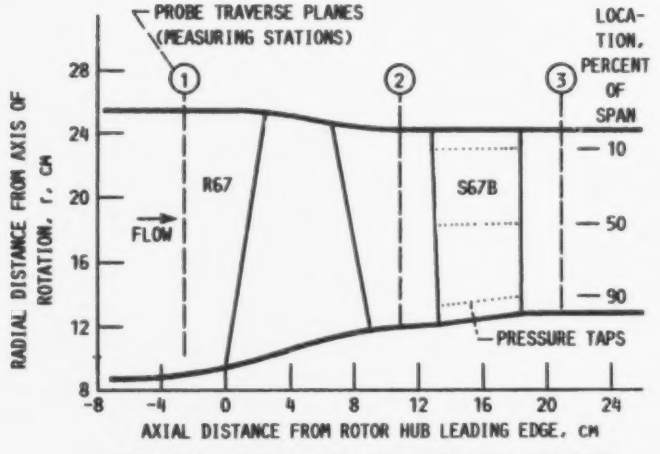

FIGURE 3. - FLOW PATH AND INSTRUMENTATION LOCATIONS.

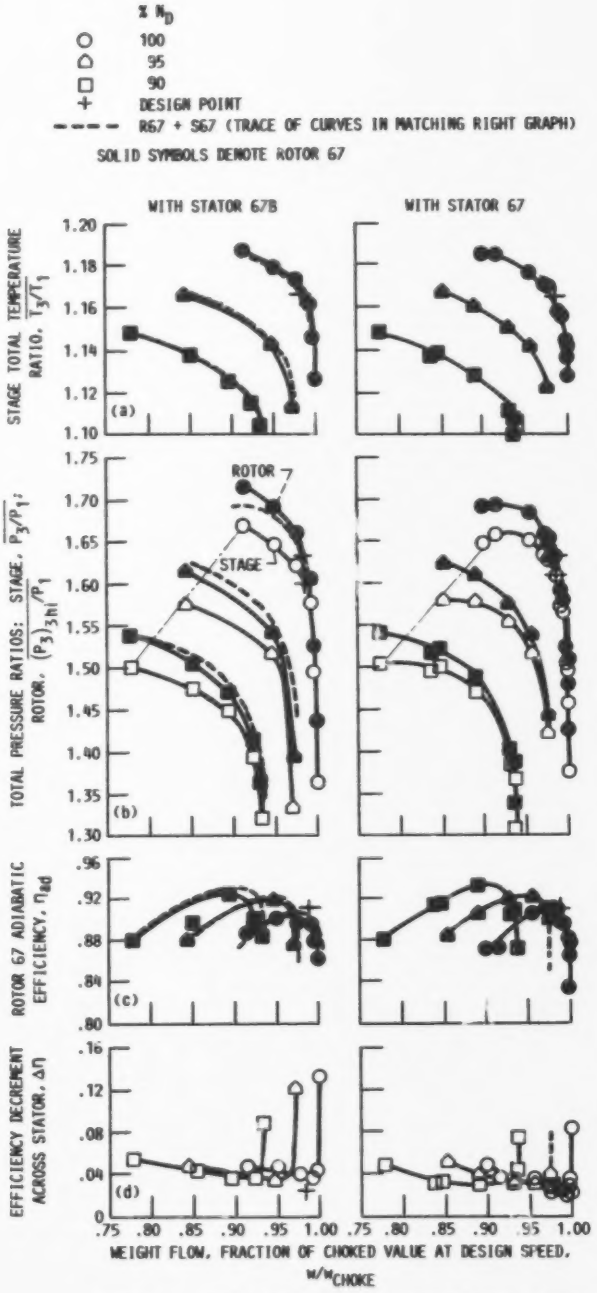

FIGURE 4. - OVERALL PERFORMANCE OF STAGE 67B (R67 + S67B), STAGE 67 (R67 + S67), AND ROTOR 67. WEIGHT FLOW WITH STAGE CHOKED AT DESIGN SPEED, w_{CHOKE}, 35 KG/SEC.

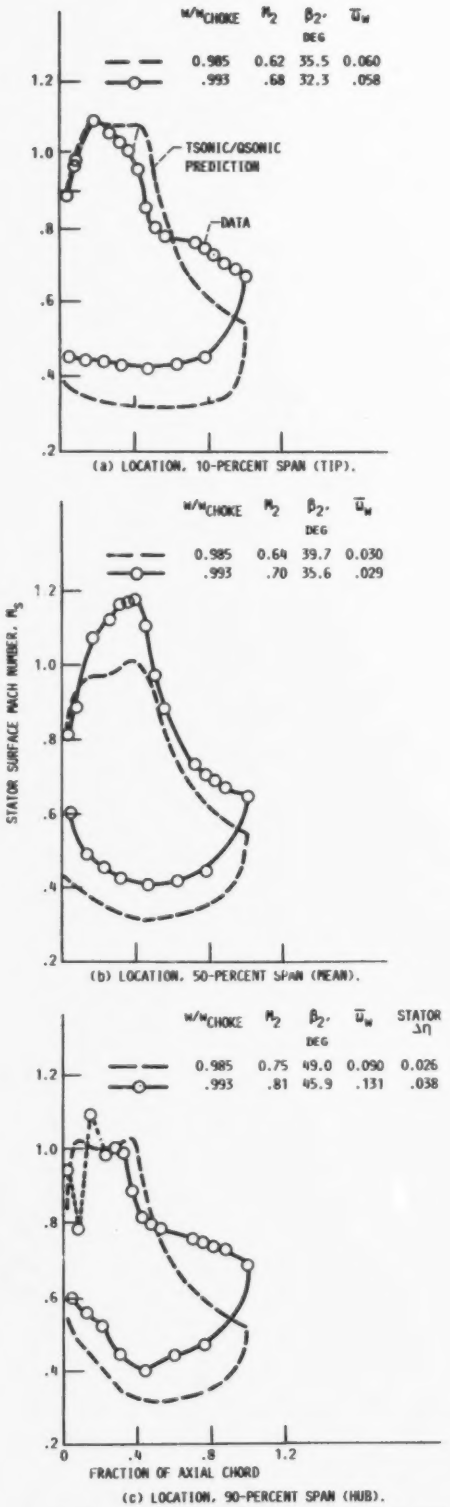
w/w_{CHOKE} M_2 β_2, DEG $\overline{u}_w$
0.985 0.62 35.5 0.060
.993 .68 32.3 .058
TSONIC/QSONIC PREDICTION
DATA
(a) LOCATION, 10-PERCENT SPAN (TIP).
w/w_{CHOKE} M_2 β_2, DEG $\overline{u}_w$
0.985 0.64 39.7 0.030
.993 .70 35.6 .029
STATOR SURFACE MACH NUMBER, M_S
(b) LOCATION, 50-PERCENT SPAN (MEAN).
w/w_{CHOKE} M_2 β_2, DEG $\overline{u}_w$ STATOR $\Delta\eta$
0.985 0.75 49.0 0.090 0.026
.993 .81 45.9 .131 .038
FRACTION OF AXIAL CHORD
(c) LOCATION, 90-PERCENT SPAN (HUB).

FIGURE 5. - SURFACE MACH NUMBER DISTRIBUTIONS AT THREE SPANS FOR STATOR 67B OPERATING NEAR MINIMUM EFFICIENCY DECREMENT ACROSS STATOR AT 100-PERCENT DESIGN SPEED.

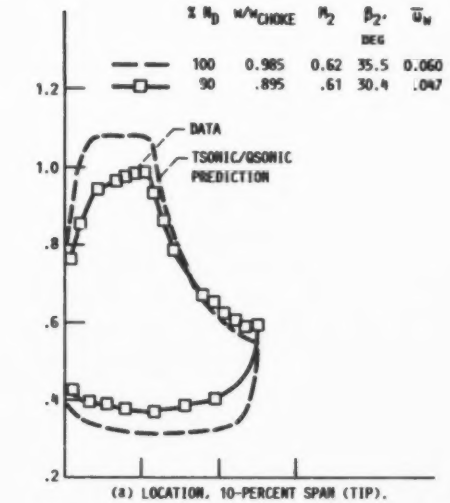

(a) LOCATION, 10-PERCENT SPAN (TIP).

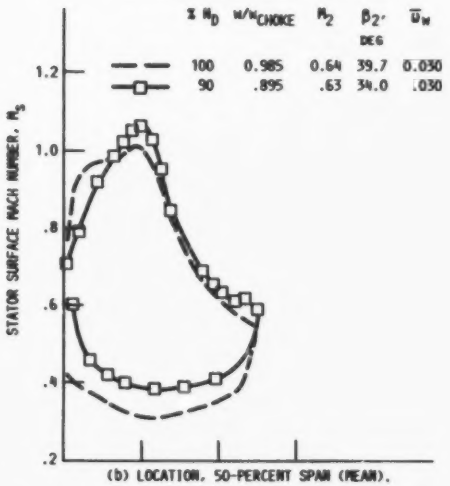

(b) LOCATION, 50-PERCENT SPAN (MEAN).

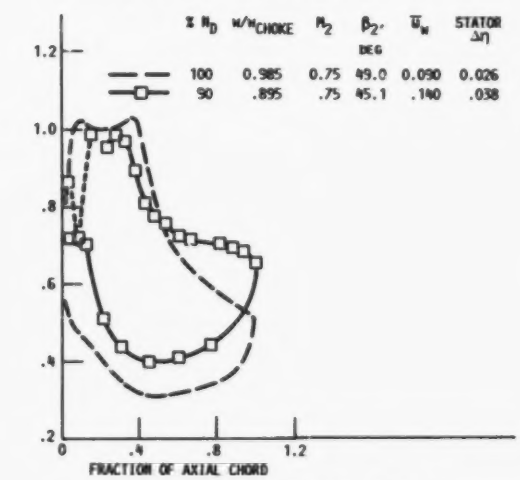

(c) LOCATION, 90-PERCENT SPAN (HUB).

FIGURE 6. - SURFACE MACH NUMBER DISTRIBUTIONS AT THREE SPANS FOR STATOR 67B OPERATING NEAR MINIMUM EFFICIENCY DECREMENT ACROSS STATOR AT 90-PERCENT DESIGN SPEED.

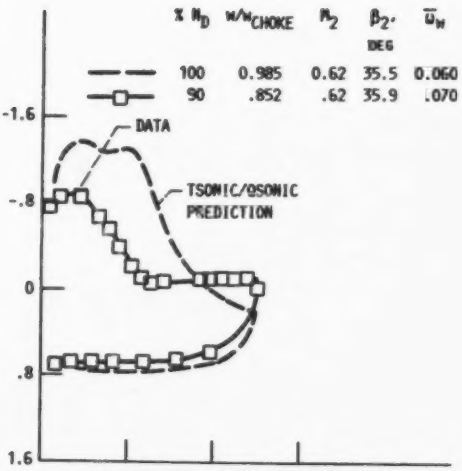

(a) LOCATION, 10-PERCENT SPAN (TIP).

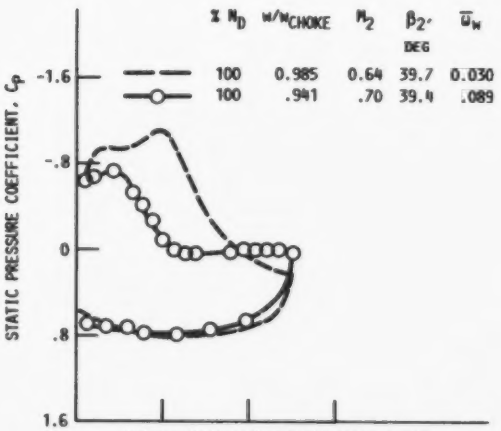

(b) LOCATION, 50-PERCENT SPAN (MEAN).

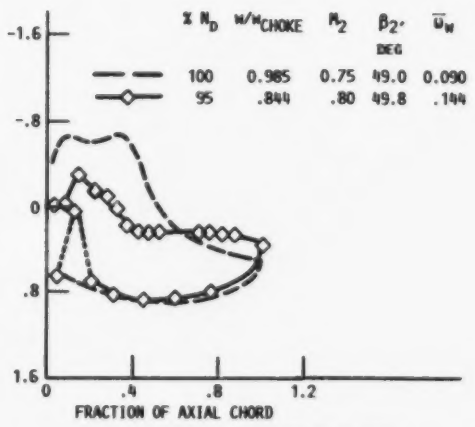

(c) LOCATION, 90-PERCENT SPAN (HUB).

FIGURE 7. - SURFACE PRESSURE COEFFICIENT DISTRIBUTIONS FOR STATOR 67B AT THREE SPANS WHEN EACH IS OPERATING NEAR ITS DESIGN INLET AIR ANGLE.

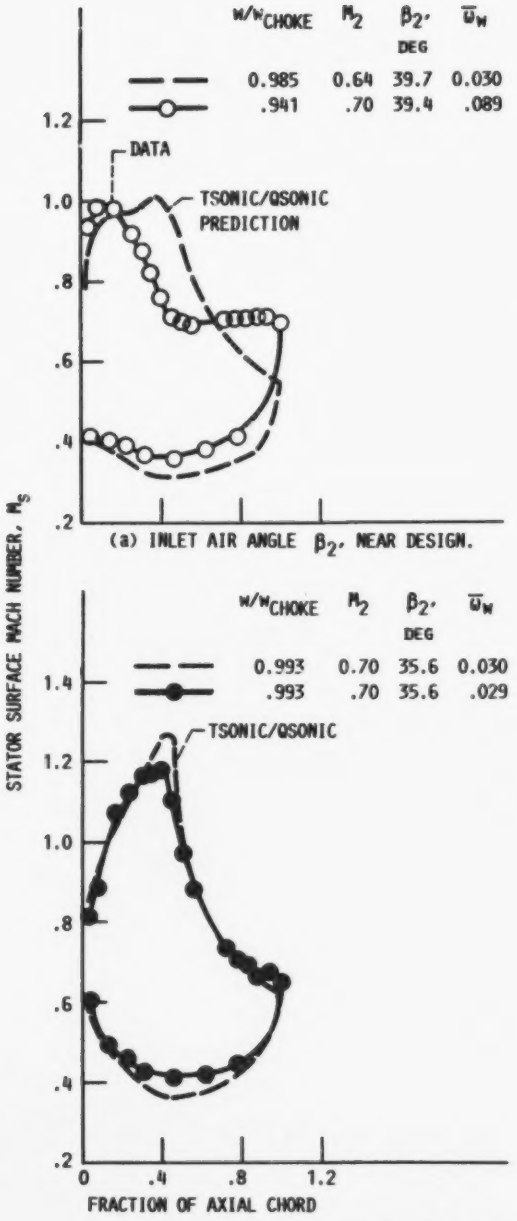

(a) INLET AIR ANGLE β_2, NEAR DESIGN.

(b) INLET AIR ANGLE β_2, NEAR MINIMUM-LOSS OPERATION.

FIGURE 8. - SURFACE MACH NUMBER DISTRIBUTIONS AT 50-PERCENT SPAN FOR STATOR 67B FOR INLET AIR ANGLES NEAR DESIGN AND NEAR MINIMUM-LOSS OPERATION AT 100-PERCENT DESIGN SPEED.

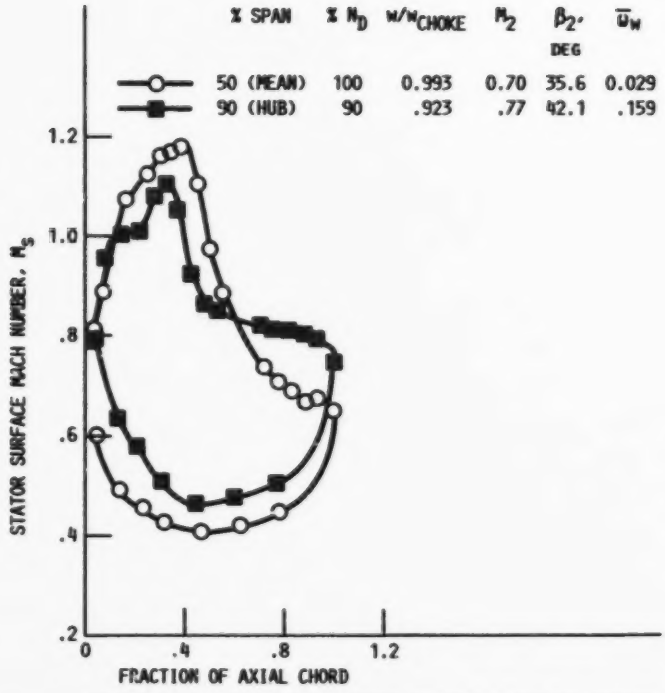

FIGURE 9. - SURFACE MACH NUMBER DISTRIBUTIONS FOR STATOR 67B SHOWING SIMILAR PATTERNS OVER FORWARD CHORD BUT DIFFERENT ONES OVER AFT CHORD.

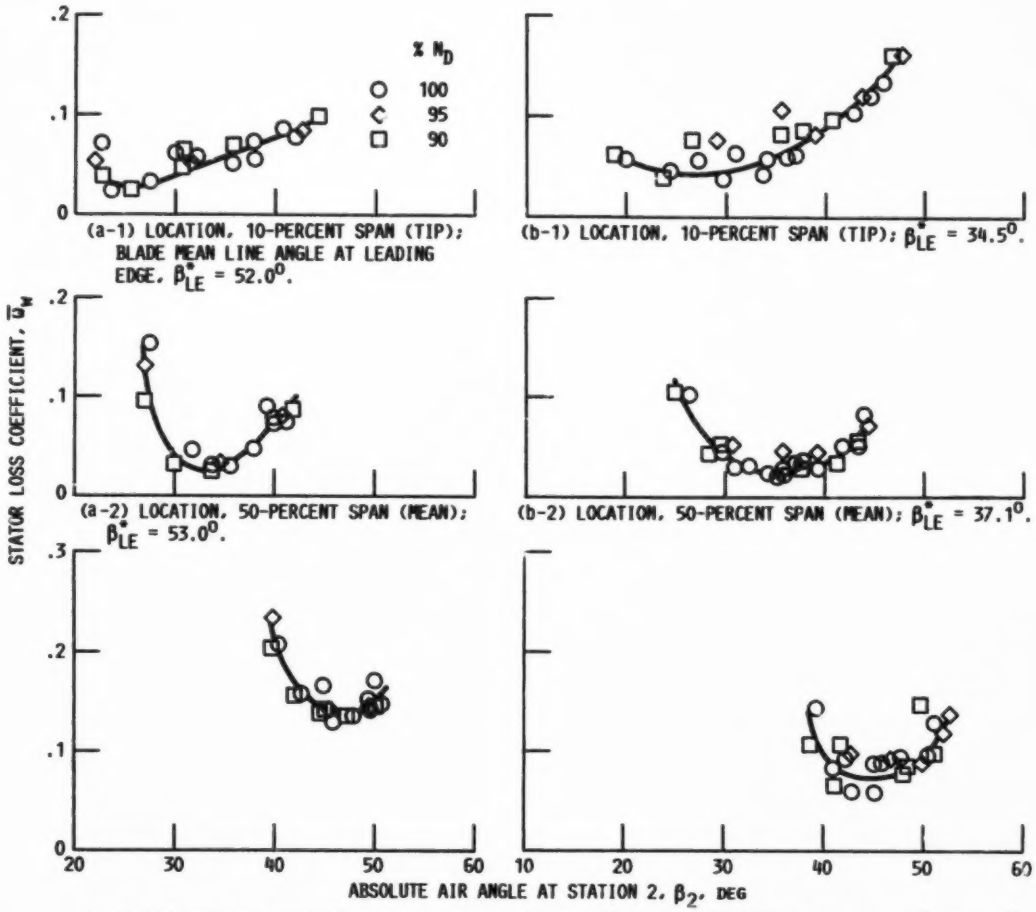
% N_D
100
95
90
STATOR LOSS COEFFICIENT, $\bar{\omega}_w$
ABSOLUTE AIR ANGLE AT STATION 2, β_2, DEG
(a-1) LOCATION, 10-PERCENT SPAN (TIP); BLADE MEAN LINE ANGLE AT LEADING EDGE, $\beta^*_{LE} = 52.0^0$.
(b-1) LOCATION, 10-PERCENT SPAN (TIP); $\beta^*_{LE} = 34.5^0$.
(a-2) LOCATION, 50-PERCENT SPAN (MEAN); $\beta^*_{LE} = 53.0^0$.
(b-2) LOCATION, 50-PERCENT SPAN (MEAN); $\beta^*_{LE} = 37.1^0$.
(a-3) LOCATION, 90-PERCENT SPAN (HUB); $\beta^*_{LE} = 60.2^0$.
(b-3) LOCATION, 90-PERCENT SPAN (HUB); $\beta^*_{LE} = 46.1^0$.
(a) STATOR 67B.
(b) STATOR 67.

FIGURE 10. - BLADE LOSSES AT THREE SPANS FOR STATORS 67B AND 67 OVER RANGE OF INLET AIR ANGLES BETWEEN STAGE CHOKE AND STALL.

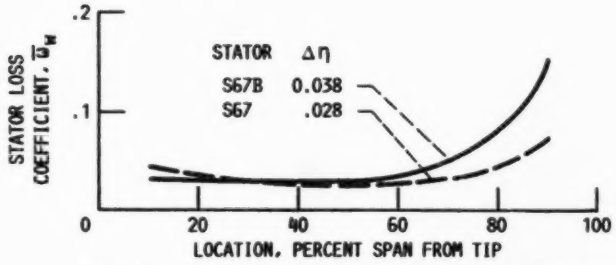

FIGURE 11. - SPANWISE DISTRIBUTION OF BLADE LOSSES FOR STATORS 67B AND 67 WHEN EACH IS OPERATING AT ITS MINIMUM OVERALL EFFICIENCY DECREMENT AT 90 TO 100 PERCENT OF DESIGN SPEED.

NASA
National Aeronautics and Space Administration

Report Documentation Page

1. Report No.	2. Government Accession No.	3. Recipient's Catalog No.
NASA TM-100141 AVSCOM TR-87-C-25		

4. Title and Subtitle
Design and Performance of Controlled-Diffusion Stator Compared With Original Double-Circular-Arc Stator

5. Report Date

6. Performing Organization Code
535-05-01

7. Author(s)
Thomas F. Gelder, James F. Schmidt, Kenneth L. Suder, and Michael D. Hathaway

8. Performing Organization Report No.
E-3694

10. Work Unit No.

9. Performing Organization Name and Address
NASA Lewis Research Center and Propulsion Directorate, U.S. Army Aviation Research and Technology Activity - AVSCOM, Cleveland, Ohio 44135

11. Contract or Grant No.

13. Type of Report and Period Covered
Technical Memorandum

12. Sponsoring Agency Name and Address
National Aeronautics and Space Administration Washington, D.C. 20546 and U.S. Army Aviation Systems Command, St. Louis, Mo. 63120

14. Sponsoring Agency Code

15. Supplementary Notes
Prepared for the 1987 Aerospace Technology Conference and Exposition, sponsored by the Society of Automotive Engineers, Long Beach, California, October 5-8, 1987. Thomas F. Gelder, James F. Schmidt, and Kenneth L. Suder, NASA Lewis Research Center; Michael D. Hathaway, Propulsion Directorate.

16. Abstract
The capabilities of two stators, one with controlled-diffusion (CD) blade sections and one with double-circular-arc (DCA) blade sections, were compared. A CD stator was designed and tested that had the same chord length but half the blades of the DCA stator. The same fan rotor (tip speed, 429 m/sec; pressure ratio, 1.65) was used with each stator row. The design and analysis system is briefly described. The overall stage and rotor performances with each stator are compared, as are selected blade element data. The minimum overall efficiency decrement across the stator was approximately 1 percentage point greater with the CD blade sections than with the DCA blade sections.

17. Key Words (Suggested by Author(s))	18. Distribution Statement
Controlled-diffusion stator Turbomachinery	Unclassified - unlimited Subject Category 07

19. Security Classif. (of this report)	20. Security Classif. (of this page)	21. No of pages	22. Price*
Unclassified	Unclassified	21	A02

NASA FORM 1626 OCT 86

*For sale by the National Technical Information Service, Springfield, Virginia 22161